Materials Science & Engineering A 766 (2019) 138391

Contents lists available at ScienceDirect

Materials Science & Engineering A

journal homepage: www.elsevier.com/locate/msea

Hot ductility behavior of AD730™ nickel-base superalloy

Seyedmohammad Tabaie[a,*], Davood Shahriari[a], Cléa Plouze[a], Alexandre Devaux[b], Jonathan Cormier[c], Mohammad Jahazi[a,**]

[a] Department of Mechanical Engineering, École de Technologie Supérieure (ÉTS), Montreal, QC, Canada
[b] Aubert & Duval, Site des Ancizes, BP1, 63770, Les Ancizes Cedex, France
[c] Département de Physique et Mécanique des Matériaux Institut Pprime, CNRS-ENSMA-Université de Poitiers, UPR, CNRS, 3346, Futuroscope-Chasseneuil Cedex, France

Authors' accepted manuscript
Article published in *Materials Science and Engineering: A*, Volume 766, 24 October 2019, 138391
https://doi.org/10.1016/j.msea.2019.138391

Authors' accepted manuscript
Article published in *Materials Science and Engineering: A*, Volume 766, 24 October 2019, 138391
https://doi.org/10.1016/j.msea.2019.138391

Hot Ductility Behavior of AD730™ Nickel-base Superalloy

Seyedmohammad Tabaie* [a], Davood Shahriari [a], Cléa Plouze [a], Alexandre Devaux [b], Jonathan Cormier [c], Mohammad Jahazi* [a]

[a] Department of Mechanical Engineering, École de Technologie Supérieure (ÉTS), Montreal, QC, Canada
[b] Aubert & Duval, Site des Ancizes, BP1, 63770 les Ancizes Cedex, France
[c] Département de Physique et Mécanique des Matériaux Institut Pprime, CNRS-ENSMA-Université de Poitiers, UPR CNRS 3346 Futuroscope-Chasseneuil Cedex, France

Abstract

Hot ductility of the newly developed AD730™ nickel-base superalloy was investigated in the temperature interval 1050-1240°C. The nil strength and nil ductility temperatures were determined by hot tensile testing using the Gleeble™ 3800 weld thermal simulation method. The influence of heating rate, representing the weld thermal cycle, on hot ductility behavior of the alloy was also investigated. The microstructure and the fracture mode of samples were examined by optical and scanning electron microscopy. The influence of heating rate on the extent of grain boundary liquation and void formation was determined and it is shown that the significant ductility loss near the NDT point could be related to the reduction of surface tension at the grain boundary-matrix interface. In addition, the contribution of hard precipitates, such as grain boundary MC carbides, voids, and cavities as other damage mechanisms responsible for ductility loss at high temperature, are discussed.

Keywords: Hot Ductility Test; Nil Ductility Temperature; Nil Strength Temperature; Void Formation; Liquation.

1. Introduction

Investigations on hot-ductility behavior of materials are used to evaluate the susceptibility of an alloy to cracking at elevated temperatures, during solidification, hot deformation, or welding [1]. Considering that nearly all engineering alloys go through the above manufacturing processes; it is therefore of critical importance to quantify and better understand their hot ductility behavior. Nil ductility temperature (NDT) and nil-strength temperature (NST) are two key parameters when studying the hot ductility of metallic systems [2, 3]. NDT has been defined as the temperature at which the material experiences significant ductility drop (e.g. reduction in area) during tensile testing and NST is the temperature at which the alloy, under the effect of a very

*Corresponding author.
E-mail address: Seyedmohammad.tabaie.1@etsmtl.net
E-mail address: Mohammad.Jahazi@etsmtl.ca

small constant tensile load, loses its strength [2, 3]. NST is located in the temperature interval between the NDT point and the liquidus temperature (T_L) and corresponds to the point where the alloy loses its strength [4-6].

Segregation of solutes and formation of precipitates along grain boundaries have been identified as the main causes of ductility loss at high temperatures [7-12]. Therefore, alloy systems with a large number of alloying elements in their composition and microstructure are prone to hot cracking. Superalloys, as the most performant high temperature alloys, and particularly modern nickel-based superalloys have sometimes up to fifteen alloying elements in their composition and several types of precipitates and are therefore highly sensitive to hot cracking during forging or Heat Affected Zone (HAZ) liquation cracking of welded structures [1, 13-17].

Mejia et al. [10] observed that hot ductility of an advanced high strength steel (AHSS) was mainly controlled by deformation induced matrix and grain boundary sliding by formation of the thin pro-eutectoid ferrite layer and the precipitation of carbides or nitrides particles at the austenite grain boundaries. Lee et al. [18] reported that the severity of the ductility loss of a GTD111 and Inconel 738LC (IN738LC) superalloys were dependent on the degree of grain boundary wetting due to constitutional liquation of MC carbide precipitates. Qian and Lippold determined NDT and NST points of Inconel 718 (IN718) [14] and Waspaloy [17] and reported that MC-type carbide constitutional liquation and segregation induced grain boundary liquation are responsible for HAZ liquation cracking behavior. They considered that the grain size and grain boundary characteristics are the two primary factors influencing HAZ liquation cracking. Knock et al. [19] studied the weldability of IN718 and the fracture surfaces of samples after NDT and NST. They observed many carbides and voids in fracture surface which caused failure at NDT and NST points. Ramirez [13] reported on Inconel 740 susceptibility to liquation cracking and ductility-dip cracking and found NDT and NST for the alloy. Anderson et al. [11] investigated the hot ductility of Haynes 282 alloy using low heating rates with different solution heat treatments conditions. They found that the on-heating ductility drop occurred because of liquation of secondary phases and melting point depressant elements for all the applied heating rate. However, in the above studies, most, if not all, the heating rates used for the investigations were very low and are not well representative of the heating rates encountered during real welding conditions (100-400°C/s [20-23]), whether solid state such as Linear Friction Welding (LFW) or fusion welding.

In recent years with the advent of new manufacturing technologies, LFW has been considered as a very competitive technology for producing blade integrated disks (Blisks) compared to the conventional fir-tree disk-blade mechanical assembly [24-26]. LFW is a solid state joining process during which through the generation of frictional heat and application of a forge pressure, the mating interface is brought to high temperature, high strain plastic deformation (1-20 s^{-1}) [20-23], and welded together. Despite the fact that no melting is expected to occur at the interface; however, due to the large number of alloying elements in the composition of

superalloys, liquation cracking could occur under some processing conditions resulting in significant ductility loss and produce unacceptable weld defects or even fracture. Specifically, weld regions between the HAZ and the weld line are prone to crack susceptibility due to possible liquation or void formation as a result of rapid and uneven thermal cycles [27].

In the present work, the influence of some LFW process parameters (high temperature and high heating rate) on hot ductility behavior of a new generation nickel-based superalloy, AD730^{TM} intended for Blisk applications will be investigated. Specifically, the NDT and NST temperatures were determined, the fracture surfaces of the samples were examined and possible governing mechanisms for the observed behaviors are discussed. It should be mentioned that despite the above mentioned studies on hot ductility loss of superalloys, few or none of them consider conditions similar to the ones observed during LFW and very few of them correlate the NDT and NST temperatures with the fracture surface of the alloy.

2. Materials and Experimental Methods

The AD730^{TM} alloy was provided by Aubert & Duval. The alloy was produced through ingot casting using vacuum induction process followed by vacuum arc remelting and finally radial forging to produce a bar-round billet with a diameter of 86 mm (Fig. 1). An 84 mm in diameter and 110 mm in length bar was then cut from the center of the billet for the study. The bar was solutionized at 1080 °C for four hours followed by air cooling.

The chemical composition of the studied material is given in Table 1. The microstructure of the alloy is shown in Fig. 2 with an average grain size of 51.36 ± 9.14 µm and γ' volume fraction of 40% [28, 29].

Table 1. Chemical composition of AD730™.

Element	Ni	Fe	Cr	Co	Al	Ti	Mo	W	Nb	C
Wt. %	Bal.	4	15.8	8.0	2.4	3.8	2.9	2.0	1.2	0.02
At. %	Bal	4.08	17.31	7.73	5.07	4.52	1.72	0.62	0.74	0.094

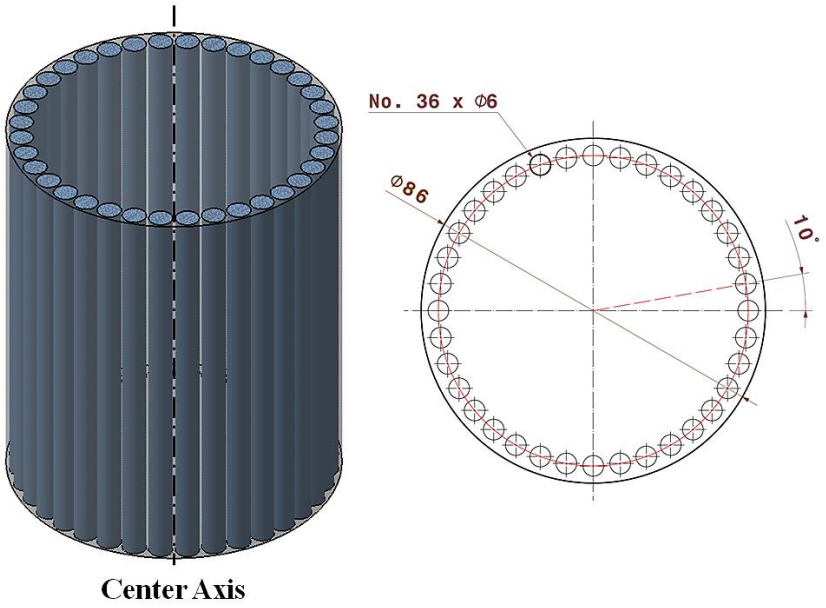

Figure 1. NDT and NST sample location in the as forged billet.

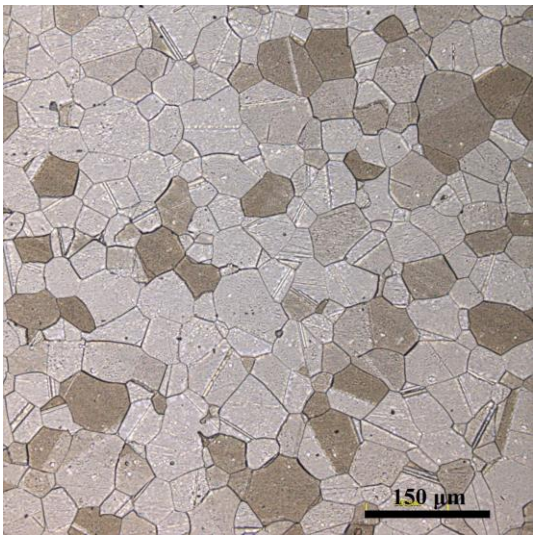

Figure 2. Initial microstructure of AD730™ superalloy.

For NST and NDT experiments, 10 mm diameter and 120 mm long rods were prepared from the external diameter of the bar using electro discharge wire cut machining (wire-EDM). Figure 1 displays a schematic view of the bar and the location of the machined rods along with their dimensions.

The determination of the NDT and NST temperatures was made using the Gleeble™ 3800 thermomechanical simulator. Heating rates in the range, 5-100°C/s in the temperature interval of 1050-1240°C and a strain rate 2.5 s^{-1} were used for the test, which were all carried out under vacuum. The thermal cycle consisted of two distinct steps: the heating and the cooling cycle. In

the heating step, the heating rate, the peak temperature, and the holding at peak temperature were controlled with high precision (less than 0.2% variation) using the advanced control system of the Gleeble machine. During the cooling step, cooling rate and holding time at test temperature needed to be precisely controlled. A pair of specially designed grips was used in order to increase the accuracy of the results during testing and reduce to a minimum the temperature gradient along the sample gauge length.

Two series of tests with different sample geometries and experimental setup was conducted for the determination of the NST and NDT. For NST tests, 75 mm long and 6 mm diameter samples were used in a setup in the Gleeble^{TM} system as shown in Figure 3. A pneumatic actuator equipped with the nil strength jaw system was employed to apply a nominal tensile loading of 90 N. This small load was applied before heating and was kept constant throughout the test until the fracture of the specimen. R-type thermocouple wires were welded within the span zone, in the middle of the sample. Samples were then heated in vacuum at 10^{-6} torr using alternated current with heating rates of 5°C/s, 25 °C/s, 50 °C/s, and 100 °C/s until rupture. The measured temperature at the rupture point is the NST of the alloy.

For the NDT tests (i.e. hot ductility tests), different specimen size and geometry as well as machine setup, as schematically illustrated in Figure 4 were used. The maximum peak temperature was selected approximately 50 °C lower than the determined NST. The specimens were heated therefore to temperatures in the range 1050°C-1240°C at a constant heating rate of 100 °C/s followed by two seconds holding time before it was strained at a rate of 125 mm s^{-1} (~2.5 s^{-1}) until failure. Figure 5 shows the testing procedures used for the determination of the nil strength temperature and the hot ductility behavior of the AD730^{TM} alloy.

Both NST and NDT experiments were repeated at least three times to validate repeatability of the results and the mean value were used for subsequent analyses. The fracture area was measured after each experiment using a digital caliper as well as profilometer to ensure accuracy and the average of the readings was considered as the reduced diameter of the fractured sample. In agreement with other published works, the limit of 5% reduction area was considered as the criteria for the determination of the NDT point [2].

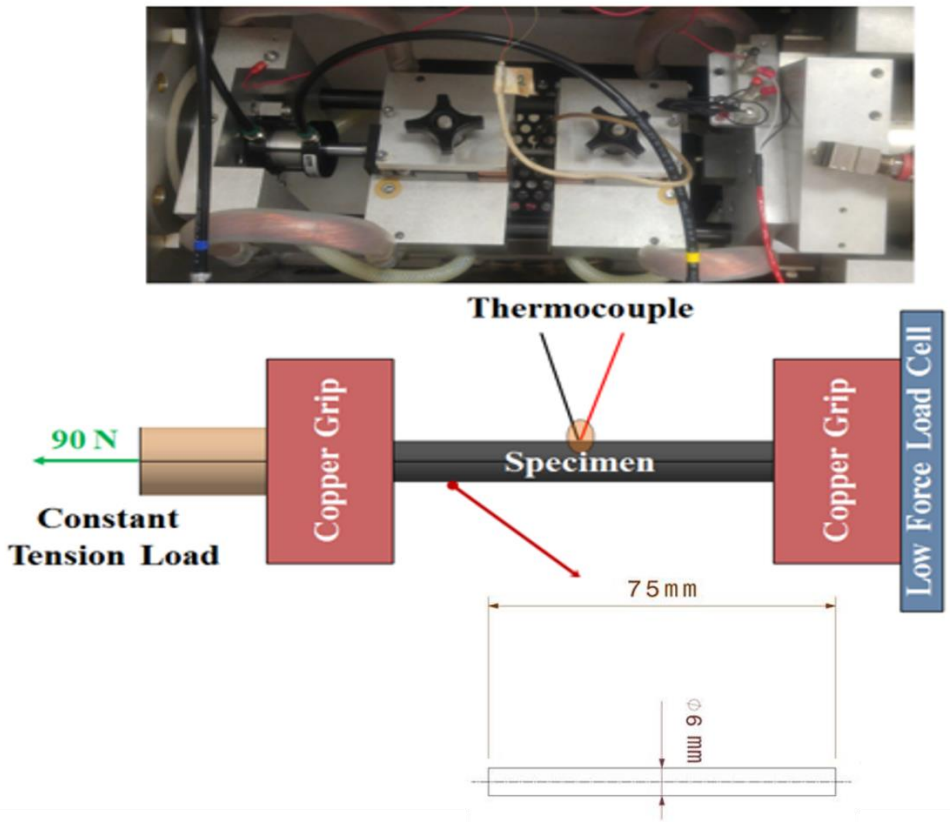

Figure 3. Gleeble™ 3800 physical simulator setup and adapted geometry for determining nil strength temperature. Using a special actuator allows maintaining a constant 90 N tensile load on sample throughout experiment. The specimen dimensions are 75 mm long and 6 mm diameter.

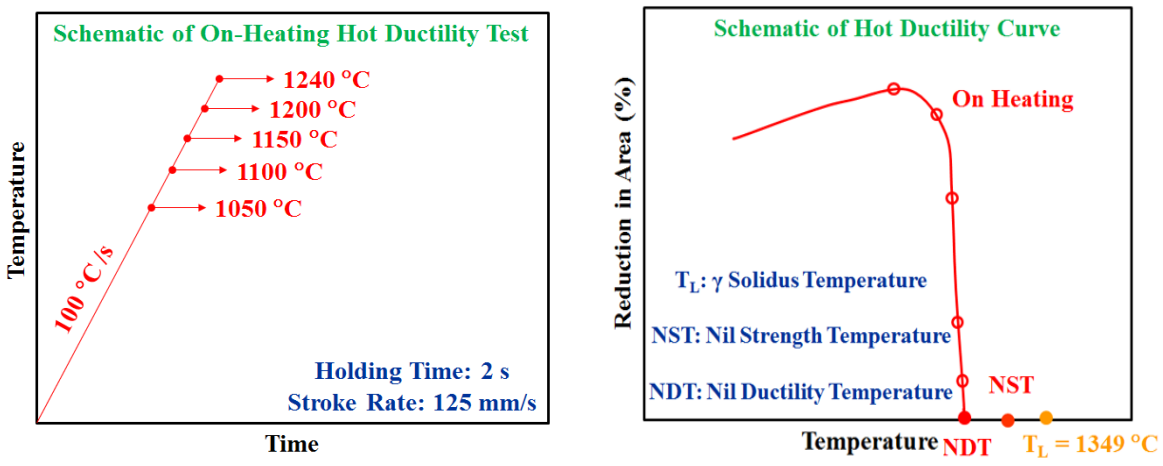

(a) (b)

Figure 4. Schematic of Gleeble™'s procedure for hot ductility testing, (a) on-heating hot tensile test with constant heating rate, holding time and stroke rate at different temperature. (b) hot ductility curve with respect to testing temperature; note that the NDT is lower than the NST and γ solidus temperature of AD730™.

The NST and NDT specimens were characterized using optical microscopy (OM) and scanning electron microscopy (SEM, TM3000, Hitachi) as well as the energy dispersive spectroscopy (EDS) technique in order to investigate fracture surface morphology, microstructural evolution, and chemical composition analysis. Examination of the NST and NDT samples was conducted in the transverse and longitudinal directions. The samples for OM and SEM observations were prepared using standard metallographic procedures and chemically etched in Kalling No.2's reagent ($CuCl_2$: 5 g, HCl: 100 ml, and ethanol: 100 ml). The growth, coalescence and fraction of voids at the fracture surface of NST samples were determined according to ASTM standard, E1382-97 [30] via images taken at 200× and 500× magnifications by OM and SEM. Digitized OM and SEM images were processed using GIMP and ImageJ software to quantify the size and fraction distribution of voids.

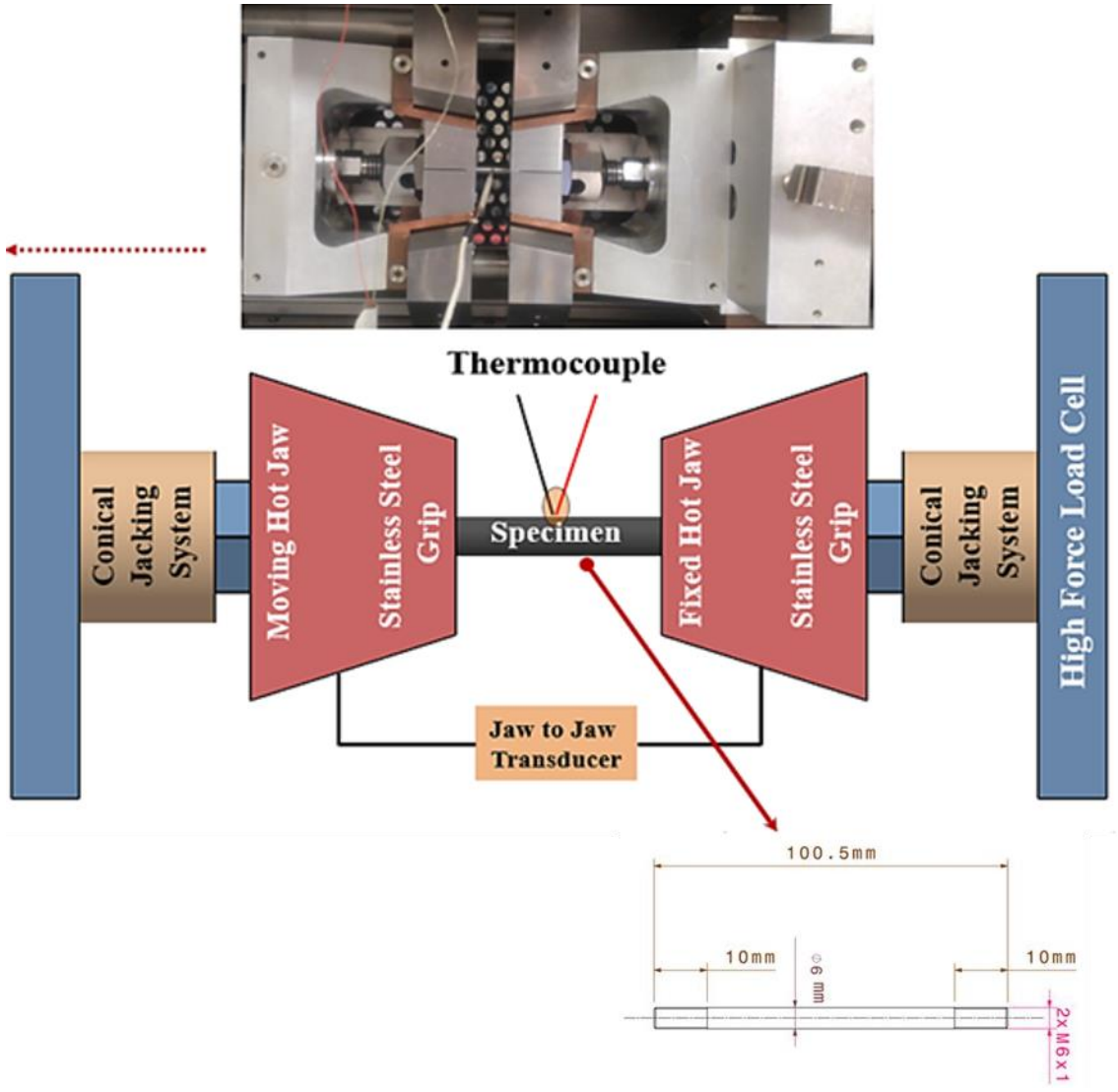

Figure 5. Gleeble™ 3800 physical simulator setup and adapted geometry for conducting hot ductility testing. Large load cell is used on the high force jaw system and the lengthwise change is controlled by longitudinal transducer.

3. Results and Discussion

3.1. Nil strength temperature

The NST was measured during on-heating experiments using four different heating rates and the obtained results were compared with the published NST of IN718 and Waspaloy [14, 31], as shown in Figure 6. The lowest NST (1280°C) was obtained for the heating rate of 5 °C/s and the highest (1295°C) for the fastest heating rate of 100 °C/s. For the intermediate heating rates of 25 and 50 °C/s the NST values were very similar varying in the range 1289°C and 1291°C. The average NST value for AD730^{TM} alloy was therefore determined to be 1290°C. The nominal temperature tolerance during all the experiments was in the range of ±1°C.

Knorovsky et al.[32] and Knock [19] reported that the average NST point for as-received IN718 for a heating rate similar of about 110 °C/s was 1276°C. Qian [31] reported an average value of 1302°C for Waspaloy in the as received condition and a heating rate of about 110 °C/s (From the literature no error bars given). It can be seen that the NST points of IN718 and Waspaloy are in the same range as the one determined for AD730^{TM}. Differences in chemical composition and applied heat treatments are probably the main reason for the observed variations in NST values between the three alloys. For instance, Boron rich constituents and grain boundary liquation were more salient in NST samples of IN718 [19, 32] and Waspaloy [31]. Furthermore, variation in heat treatment cycles may result in grain boundary segregation and/or increase the fraction of some secondary phases (e.g. δ-phase in IN718) increasing the propensity for grain boundary liquation during nil strength experiments [14, 31, 33]. On the basis of the obtained results, it could be said that the NST value does not seem to be very sensitive to the heating rate and that variations are more sensitive to chemical composition and thermal cycle applied to the alloy.

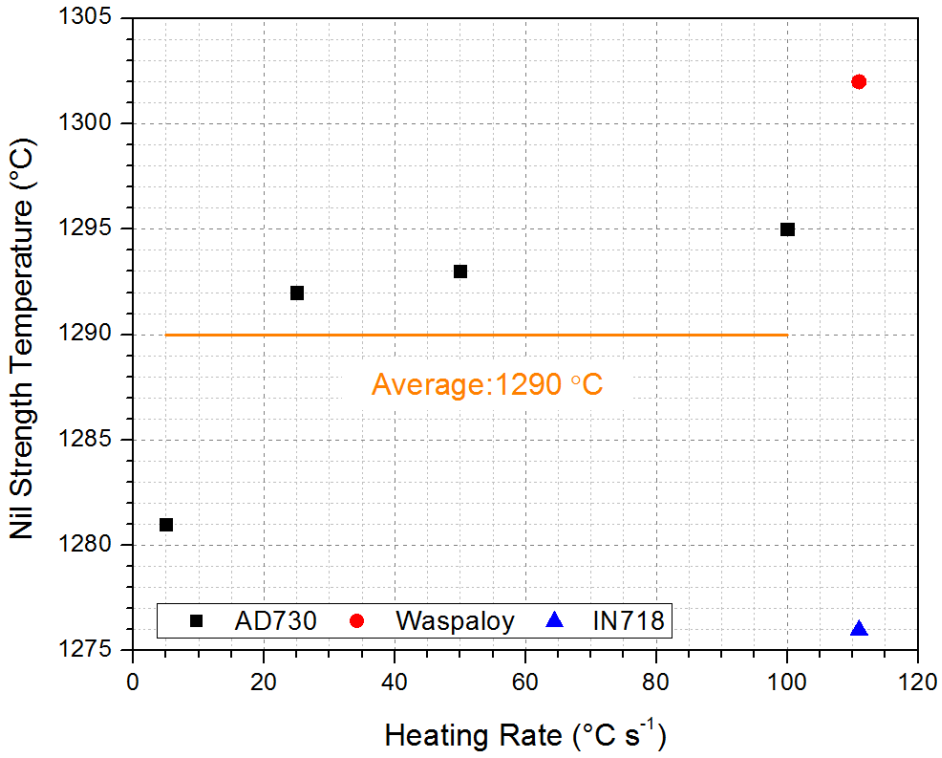

Fig. 6. Variation of the NST point of AD730™ with heating rate when compared to the NST of IN718 [19, 32] and Waspaloy [31].

3.1.1. Fracture surface analysis

Illustrative examples of the fracture surface of the NST samples are shown in Fig. 7a-d. A large number of voids were observed on the surface of the samples, as indicated by in each figure. The samples were fractured at high temperature (near to the melting point) at which the alloy had no ductility and strength. Examination of the fracture surface revealed a brittle characteristic with the presence of porosity, microvoids, and liquations for all four tested heating rates. Partial or total melting at the grain boundary was also observed in all samples, suggesting that the observed grain boundary cracks are the result of post-fracture liquid cooling. These findings corroborate with those reported by Knock in IN718 [19]. It should be noted that liquation cracking is the forming, presence and persistence of liquid films at grain boundaries (GBs) and their inability to accommodate the thermally and/or mechanically induced strain experienced during the loading at elevated temperature and weld cooling that subsequently reduce the grain boundaries strength [14, 17].

Qian and Lioppold [14] reported that in IN718 alloy, boron carbide liquation produced a low melting eutectic, an extra low melting point constituent that further aggravates the liquation then led to cracking. Masoumi et al. [34] observed liquation in AD730™ and attributed it to the melting of carbides within GBs.

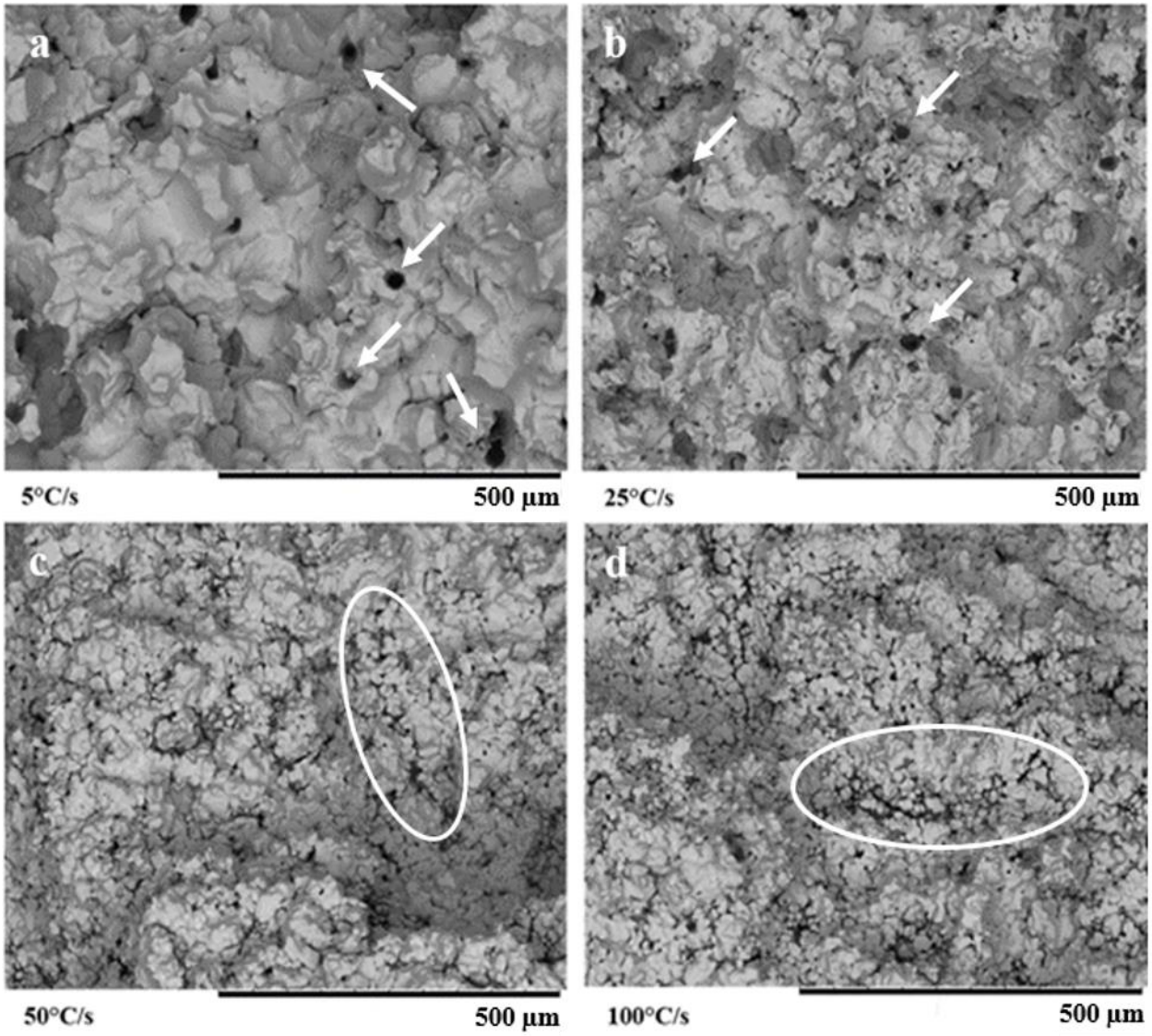

Figure 7. Fracture surface of NST samples at different heating rates. a) 5 °C/s, b) 25 °C/s, c) 50 °C/s, d) 100 °C/s. White arrows indicate the large voids and circled zones indicate small voids coalescence.

The porosities and voids observed in the above figures have been related to the application of stress during tensile test and the fracture phase through the creation of spaces as a result of grain boundary sliding or precipitate removal. Lin et al. [35] reported that interaction and accumulation of dislocations near the boundaries and particles result in strain concentration in these areas and leads to the nucleation of microvoids. In addition, the accumulation of slip bands in the boundaries causes the formation of voids; as a result, a loss of strength occurs due to decreased interface energy [36]. In the present work, the voids were counted and classified into different size categories to compare their distribution for each heating rate. Preliminary qualitative examination of the voids in different samples showed that at the heating rate of 5 °C/s (Fig. 7a), the number of microvoids is lower than the sample exposed to 100 °C/s (Fig. 7d);

however, their sizes are significantly bigger indicating the occurrence of microvoid coalescence. An intermediate trend is observed for samples heated at 25 and 50 °C/s. Figure 8 shows the evolution of void size distribution as a function of heating rate obtained by counting the voids present on the fracture surface using ImageJ image analysis software. As mentioned in the experimental method section a total number of at least 50 voids were counted for the size estimation.

As shown in Fig. 8, at higher heating rates (50 and 100 °C/s), the voids were smaller while by applying lower heating rates (5 and 25 °C/s), larger voids were formed (more than 100 µm). Considering the scatter in size distribution of the voids, they were categorized in two groups, from 0 to 10 µm and from 0 to 100 µm, and the results are shown in Figs. 9 and 10, respectively. As can be seen from these figures, a higher percentage of small voids with higher fraction could be associated to higher heating rates. In contrast, larger voids (20-100 µm) with lower fraction characterize the low heating rate conditions (5 and 25 °C/s) (Fig. 10). It should be noted that applied temperature, heating rate (i.e. time factor) and stress are the main variables that affect the extent of damage during the test. For example, NST tests are characterized with a constant stress; however, at lower heating rates, more time is available and therefore, smaller voids coalesce into one another and form larger ones that cause damage. In contrast, as shown in Fig. 9, at higher heating rates the fracture surface is characterized by a large number of small voids indicating that nucleating was accelerated but there was not enough time for void growth under these conditions. The role of temperature, time, and applied stress on the nucleation rate and growth of voids will be discussed further in the upcoming sections.

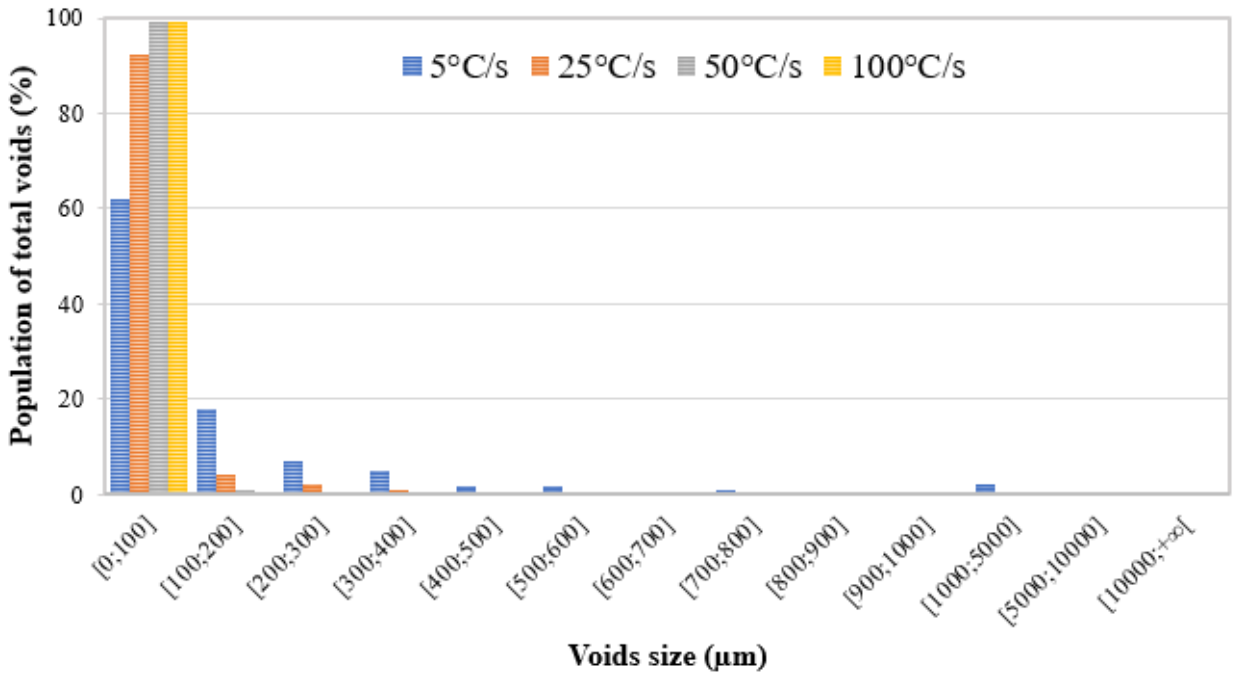

Figure 8. Voids fraction and size distribution as a function of the heating rate.

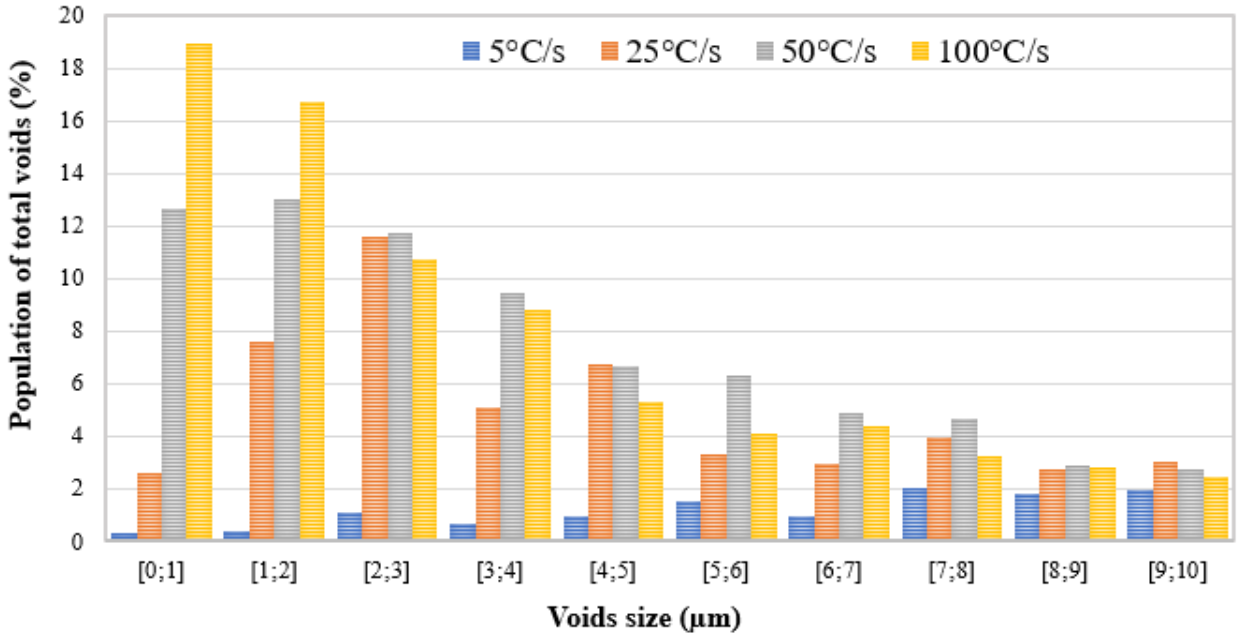

Figure 9. Distribution of void size fraction between 0 and 10 µm interval as a function of the heating rate.

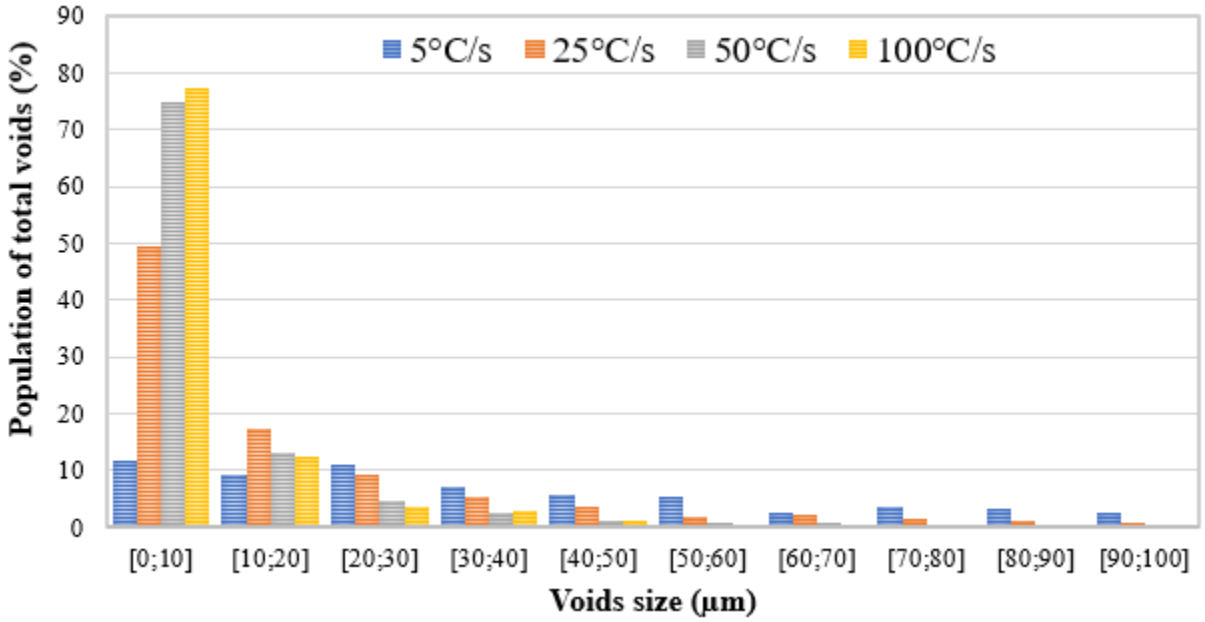

Figure 10. Distribution of void size fraction between 0 and 100 µm as a function of the heating rate.

In the case of the investigated alloy, Masoumi et al. [37, 38] observed that cavities initiated preferentially at the grain boundaries due to the nucleation of voids around the primary γ' or carbides. The NST results shown in Fig.6 indicate that even for the lowest heating rate the NST (1280°C) is above the dissolution temperature of primary γ' in AD730^{TM} (1150°C) [39]; thereby,

confirming the origin of void formation in AD730^{TM} and by extension to other nickel-based superalloys.

Finally as shown in Fig. 7(a-d), a large number of dimple like features that are visible at the fracture surface. Such surface characteristics have already been also reported in other superalloys [35, 40, 41]. They have been related to the growth (Fig 7 a and b) and coalescence of voids (Fig. 7 c and d), and cavities nucleated at grain boundaries which have been connected to the surface and assisted surface crack growth due to the reduction of the surface area resulting in the formation of a large number of microvoids that produce a dimpled crack surface [35, 40-42]. For the low heating rate, void coalescence could take place and the dimples appear larger, while for the fast heating rate very small dimples are observed at the fracture surface. Furthermore, in general, surface tension decreases when temperature increases due to lower intermolecular cohesive forces between the grains [43]. As a result, the adhesion between the grains in the boundary area is weakened, resulting in void connection and the growth of micro-cracks at the boundary and subsequent failure of the sample without any ductility. Therefore, the large number and distribution of voids which brought them closer led to the crack growth and likely easier to connect to each other and brittle fracture happened.

3.2. Nil Ductility Temperature

As explained in section 2, the hot ductility tests with the objective to determine the nil ductility temperature of the alloy were conducted between 1050 and 1240°C using a heating rate of 100°C/s.

3.2.1. Analysis of the flow curves

Fig. 11 shows the stress-strain curves of hot tensile tests of AD730^{TM} superalloy for the different temperatures of deformation. The flow behaviors are significantly affected by the deformation temperature and composed of three distinct stages, work hardening, flow softening, and the final fracture stage. A peak after the strain hardening, followed by a yield drop phenomena was also observed in all the specimens. The stress difference between the upper and lower yield points was nearly the same for the first four testing temperatures. For the 1240°C, the lower yield point was not detectable due to the sample fracture under this condition. Several authors have also reported the occurrence of a yield drop phenomena during hot deformation of various types of superalloys [7, 44]. Guimaraes and Jonas [45] attributed the stress peak to dislocation locking due to short range ordering of γ' forming elements (Ti and Al) while Chamanfar et al. [46] showed that carbides can act as an additional source for dislocation locking. Recently, Zhao et al. [47] associated the yield drop to the occurrence of softening phenomena such as dynamic recovery and dynamic recrystallization (DRX). However, considering that the yield drop occurs over a very short period of time, observing microstructural variations during yield drop becomes very challenging.

In the present work and at the tested temperatures, the slow increase of flow stress after the yield drop is mainly associated with the interaction of strain hardening and softening mechanism. The results show that the strain of the alloy increased with temperature until 1150°C. High deformation temperature can promote the mobility of grain boundaries for dislocation annihilation, and thus the flow stress decreases probably due to the grain boundaries mobility, more DRX and dissolving the secondary phase precipitates at temperatures higher than 1000°C in AD730^{TM} as reported by Masoumi et al. [37, 39]. Consequently, with increasing strain, diffuse necking occurred during tensile test and led to sample fracture. Huang et al. [48] studied the failure behavior of IN718 superalloy and observed localized necking in the temperature range above 950°C. They also found that cavitation was the main cause of localized necking, particularly at higher strain rates (strain rates above 10^{-2} s^{-1}). Therefore, the combined effects of localized necking and microvoid coalescence and interlinkage (near the NST) appear to be the responsible mechanisms for intergranular and fracture of the hot tensile tested samples.

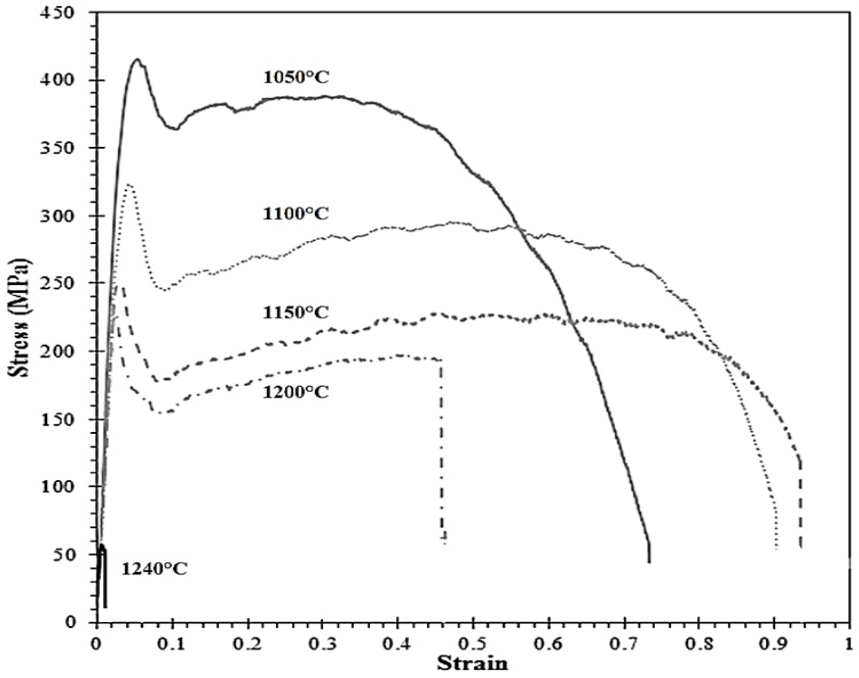

Figure 11. Stress-strain curves of hot tensile tests obtained by Gleeble™ 3800.

Fig. 12 shows the evolution of the reduction in area with temperature obtained from the hot ductility tests. Based on the defined criteria for the NDT (point of 5% reduction area) the nil ductility temperature for AD730^{TM} alloy is 1234°C. This value is in agreement with those obtained by other researchers for IN718 (1200°C) [19], IN718Plus™ (1150°C) [49], and Waspaloy (1250°C) [31]. As a result, by comparing the reported results for other alloys with the investigated alloy, it can be concluded that the difference between NST and NDT for all the above alloys is in the range of 40 to 90°C.

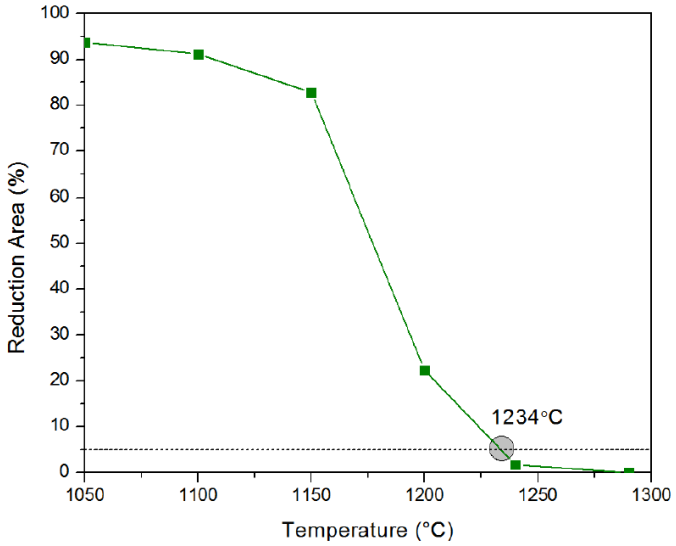

Figure 12. Hot ductility behavior during heating process at different temperatures. The standard deviation on the estimated reduction of area values is less than 2%.

A comparison of the initial microstructure of the alloy (Fig. 2) with the one after the tensile test (for 1240°C) revealed that the grains size behind the fracture zone did not change significantly passing from 51.36 ± 9.14 μm in the base material to 58.13 ± 15.43 μm (not shown here) for the samples exposed at 1240°C. This is probably related to the limited time available for grain coarsening associated with the high strain rate and heating rate used in the experiments. Therefore, the effect of grain size variation on the hot ductility behavior of the alloy under these conditions could not be significant. Furthermore, above 1150°C, the dissolution of γ′ particles and carbides in the microstructure, especially the ones at the grain boundaries, have a detrimental effect on mechanical properties as observed in the stress-strain curves of the samples tested at 1200 and 1240°C.

The results obtained in the present work show (Fig. 12) that AD730^{TM} superalloy has zero ductility under tensile loading above 1234°C, where γ′ precipitates are completely dissolved and liquation could occur under non-equilibrium conditions. Similar results have been reported by Ola et al. [50] for IN738LC. Specifically, the authors reported that the occurrence of liquation in the vicinity and within grain boundaries degraded the ductility of the alloy under tension and, as such, the alloy failed without plastic deformation [50]. Furthermore, as reported by other investigators [34, 37, 40], complete dissolution of γ' particles in the matrix of AD730^{TM} occurred at 1200ºC which resulted in significant weakening of the grain boundaries in which liquation could occur. In general, intergranular cracking at high temperatures takes place at locations with localized stress or structural imperfections such as the grain boundary edges, triple points, and interface of brittle particles and are accompanied with grain boundary slipping and the formation voids [36, 51, 52]. The possible operation of the above mechanisms in the present study will be discussed in the following.

Fig. 13 shows the fracture surface for the specimens exposed to 1050, 1100, 1150, 1200, and 1240°C. A ductile fracture characterized with a large number of dimples and interstitial cavities (Fig.13 a-c). The presence of the larger voids may be due to the presence of large precipitates such as carbides that can be seen on the fracture surface of Fig. 15. By increasing the temperature to 1200°C and then to 1240°C the fracture mode changed from intragranular to intergranular (Fig. 13d and e); however, the fracture is fully intergranular at 1240°C. The presence of cracks along the grain boundaries and the clear definition of the grain limits in the fracture surface, and the differentiation of the shape of each grain during failure are signs of (quasi-)brittle fracture. The morphology of the fracture surface and the amount of reduction area for each specimen clearly revealed the transition from ductile to brittle fracture. The evolution of the fracture surface from 1050°C to 1240°C in Fig. 13 indicates that microvoids and cavities are present along the tensile direction of the specimen and coalesce to become a continuous crack. The brittle fracture occurred when the temperature approached the NDT, whereas at lower temperatures the fracture was ductile.

The presence of grain boundary cracks and cavities within the microstructure is also reported in the zones below the fracture surface as shown in where cavities and microvoids formed due to the particle detachment (MC carbides) in the boundary areas can be observed. Fig. 14 (b) shows the formation of microcracks as a result of interconnection of previously formed cavities within the boundaries. Similar results have been reported also by Gifkins [53] and Greenwood [54]. The above findings further confirm that cavitation and void nucleation and their growth during deformation at high temperatures are the main causes for grain boundary cracking and subsequent minimum ductility.

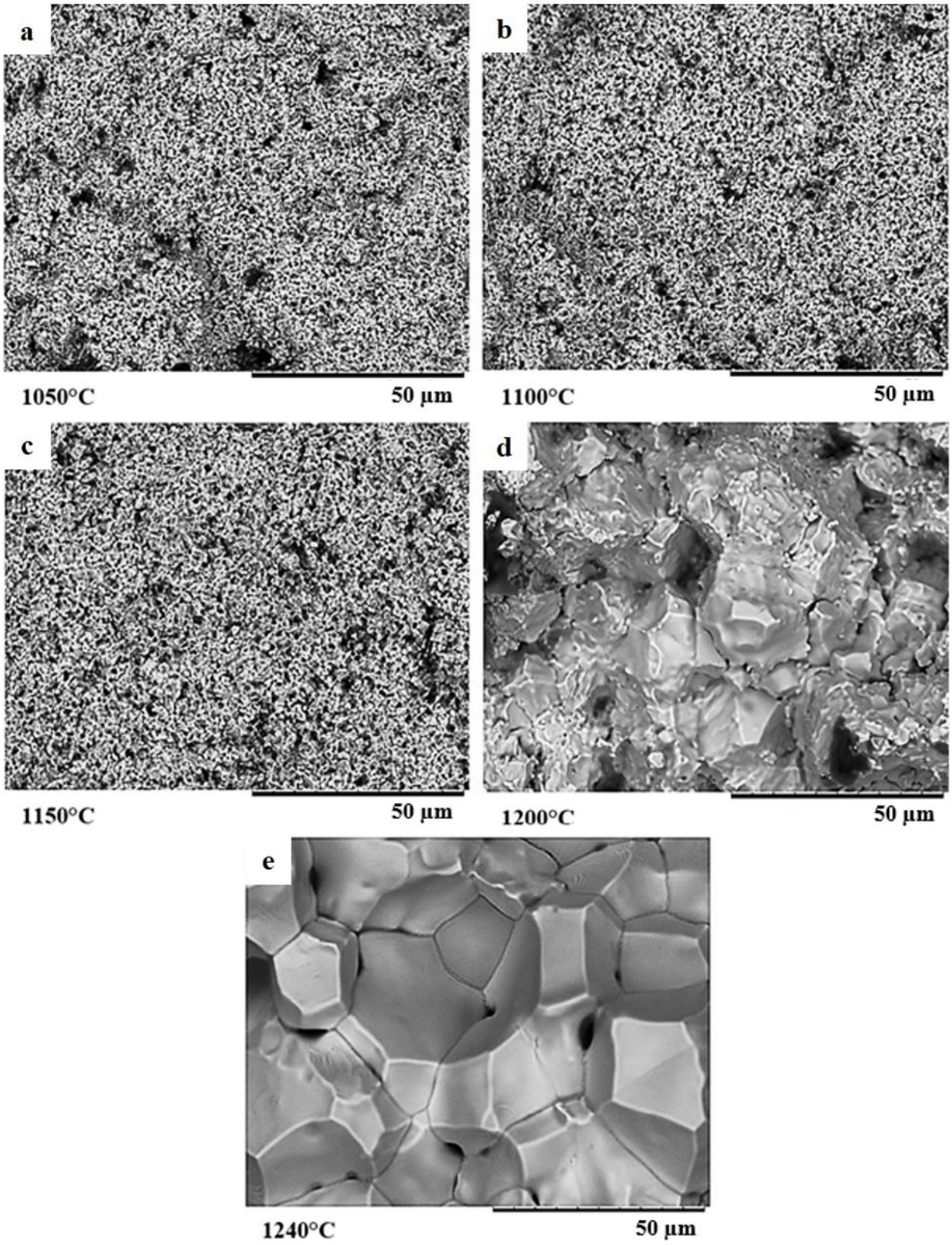

Figure 13. Fracture surface after NDT tests of AD730™ alloy, a) 1050°C, b) 1100°C, c) 1150°C, d) 1200°C, e) 1240°C.

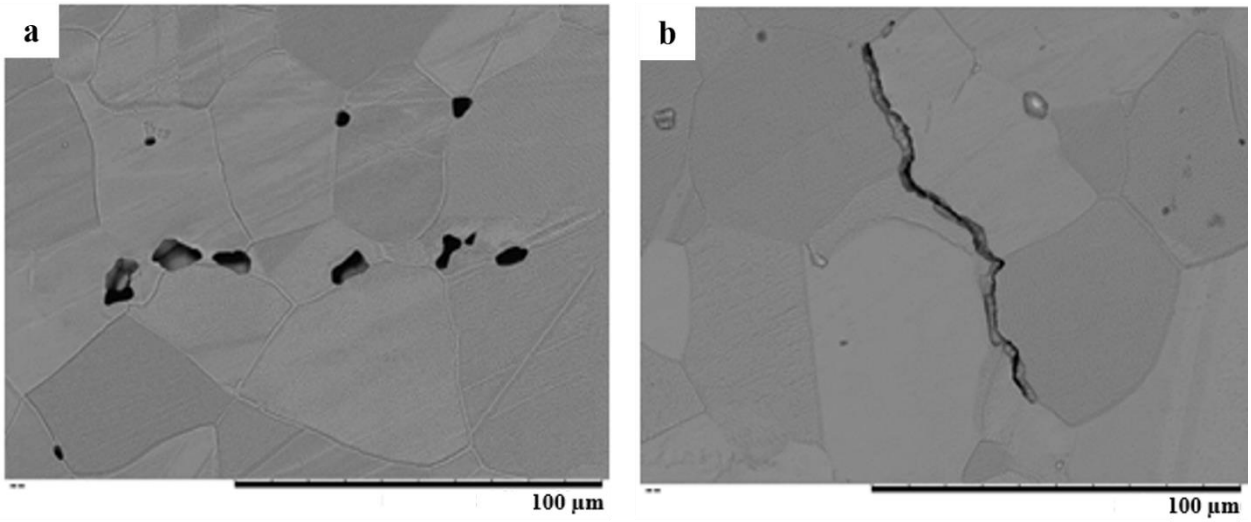

Figure 14. SEM images showing void formation and crack growth at grain boundaries in the fracture area obtained from cross-sectioned 1240°C specimen.

3.2.2. Characteristics and formation mechanism of cavities

Cavities or voids formed at grain boundaries can have different shapes depending on whether they formed at the junction of two grains, triple junctions, and four-grain junctions (voids in inclusion-free boundaries) or at the interface of inclusions or precipitates present at the grain boundaries [12, 55]. All the above type of voids and cavities were observed in the examined fracture surface of samples as shown in Figs. 13 and 15, and internal microstructure, as shown in Fig. 14.

Gifkins [53] and Smith [56] reported that the spacing between the cavities was about the same as that of the slip bands formed during the hot deformation process. Afterward, the slip bands formed ledges near the boundaries, which then nucleated the cavities through the grain boundary sliding (GBS) process by the applied stress. Moreover, cavities could also nucleate around the particles that are present at the grain boundaries [56]. As the temperature increases, the stress required to maintain a given strain-rate falls in such a way that the void growth rate increases while void nucleation rate decreases. In contrast, at low temperatures, the opposite occurs and higher nucleation rates and lower growth rates are observed [12]. The energy barrier (ΔG_c) for nucleation is function of the free surface energy (γ) or surface tension and the volume of the void of critical radius (r_c) [12]:

$$\Delta G_c = \frac{r_c^3 . F_{v(\alpha)} . \sigma}{2} \qquad \text{Eq. (1)}$$

$$r_c = \frac{2\gamma}{\sigma} \qquad \text{Eq. (2)}$$

Where σ is applied tensile stress, $F_{v(\alpha)}$ is the function of void geometry and r_c^3. $F_{v(\alpha)}$ is the volume of the void of critical size and α is the angle formed at the junction of the void and the grain boundary.

If ρ_{max} is the maximum number of potential nucleation sites in the grain boundary per unit area, then the number of critical nuclei per unit area is:

$$\rho_c = \rho_{max}.\exp(\frac{-\Delta G_c}{KT}) \qquad \text{Eq. (3)}$$

Where ρ_c is the number of supercritical nuclei formed per second and it is time-dependent. Using the above analysis the nucleation rate ($\dot{\rho}$) can be described as [12]:

$$\dot{\rho} = \frac{4\pi\gamma}{\Omega^{\frac{4}{3}}.\sigma}.D_B\delta\left(1+\frac{\sigma\Omega}{KT}\right)(\rho_{max}-\rho)\times\exp\left[-(\frac{4\gamma^3.F_{v(\alpha)}}{\sigma^2.KT})\right] \quad \text{Eq. (4)}$$

Where Ω is the atomic volume (usually $\sigma\Omega/kT \ll 1$) and $D_B\delta$ is the boundary diffusion coefficient times the boundary thickness. The exponential factor is the dominant influence in the temperature dependence of nucleation. Therefore, $F_{v(\alpha)}$, γ and σ are the critical parameters in determining the nucleation rate.

The above equation, which has been developed for pure copper, indicates that, void nucleation and growth depend on temperature; applied stress and time (i.e. strain rate and heating rate). The results obtained in the present study also confirm such dependence for the investigated nickel base superalloy. However, in order to quantitatively determine the nucleation rate of voids as a function of heating rate for AD730™ alloy, each of the variables in equation (4) need to be known. Such data (for example, void geometry, void critical radius, interface energy, etc.) is not available in the literature and their determination was out of the scope of the present study. Therefore, the time to fracture defines the area fraction of voids in a grain boundary, which could be attributed to the voids fraction and/or voids size during deformation. As different heating rates were used during the NST tests, it is expected that both void fraction and void size would vary during testing.

In general, nucleation is continuous with time i.e., the number of nuclei increases with time towards the number ρ_{max}. As shown in Fig. 15 (a) and (b), MC type carbides with M = Ti, Mo and Nb-rich carbides are present at the grain boundaries. These carbides are not coherent with the matrix and cause the formation of voids and cavities due to the difference in the shear modulus between the particles and the matrix [48, 57]. The stability of the cavity nuclei depends upon their growth to the critical size by absorbing vacancies. As reported by Gifkins and Smith [53, 56] the growth of the cavity nucleus is opposed by the cavity surface tension which tends to shrink it and suppress it, unless the cavity growth rate is high enough and could reach the critical size. Once this step is successfully passed, the cavity continues to capture vacancies until cavities

link to form *chains* [53, 56]. Finally, these chains grow to form cracks over part or all of the grain boundary and joint other cracks in the neighbouring grains (Fig. 14 (a, b)).

The presence of liquation at the grain boundaries was also observed in all samples tested at 1200 and 1240°C, as illustrated in Figure 15 (a-d). Fig. 16 shows the liquation thickness in the different zones of the sample exposed to 1240°C. As it can be seen, the average measured thickness of the liquation film within the grain boundaries is maximum in the vicinity of the fracture zone and drops significantly as the distance from the fracture surface increases. Knock [19] reported that as the liquid forms around the grains, the material retains some of its strength due to capillary effects. As the fraction of liquid increases, the capillary effects are unable to support the forces on the interface of each grain. Afterward, the surface tension diminished and the grain boundary strength decreased which led to crack growth and ductility dropped in the alloy at high temperatures. In a previous investigation on liquation in a nickel-based superalloy with relatively similar composition to AD730^{TM} , it has been reported that liquation of Cr-rich carbides (often containing some Co and W) within grain boundaries took place at the origin of the formation of the liquid zones [58].

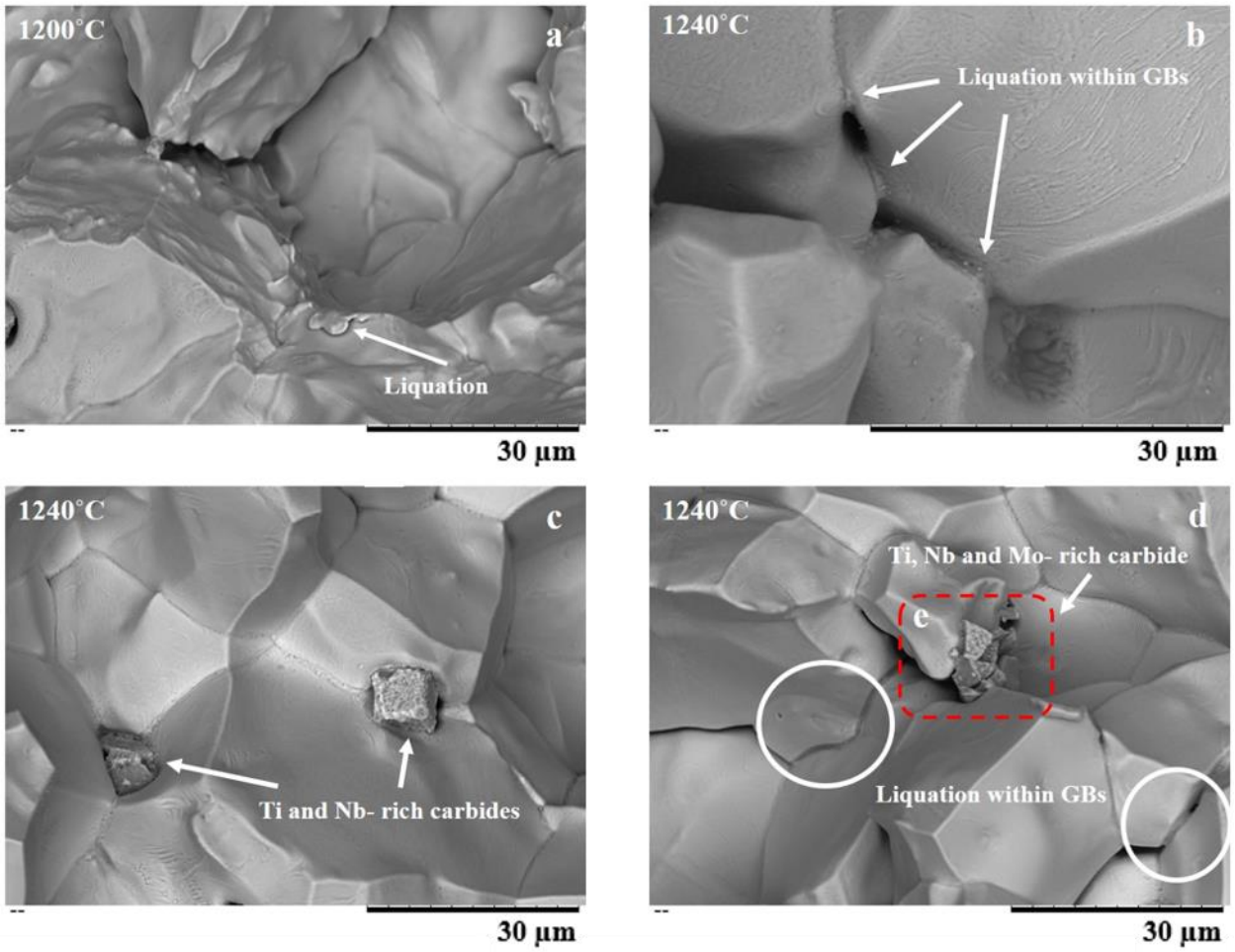

e

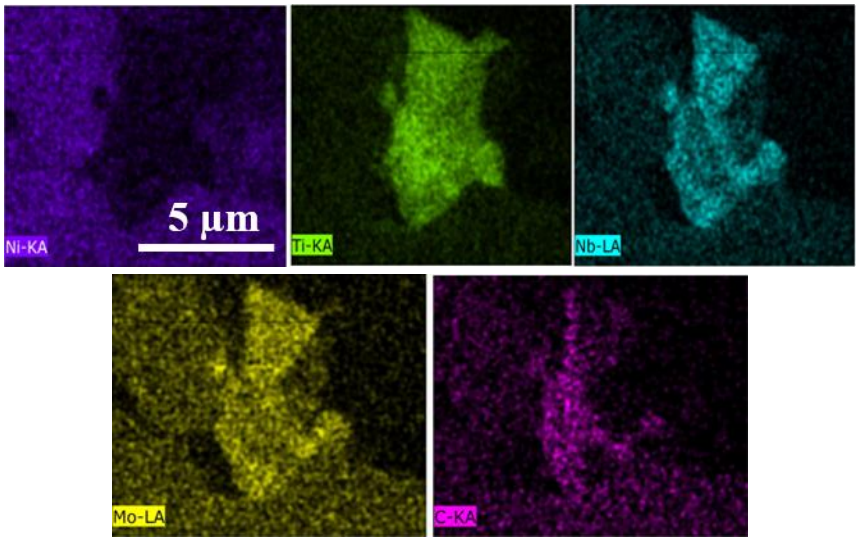

Figure 15. SEM images from samples exposed to 1200 and 1240°C of AD730™ showing: a) liquation at the GB, b) GB liquation and joining of the voids, c) carbides at GB and triple junctions, d) liquation at GB and crack growth, e) map analysis of a carbide particle in image (d).

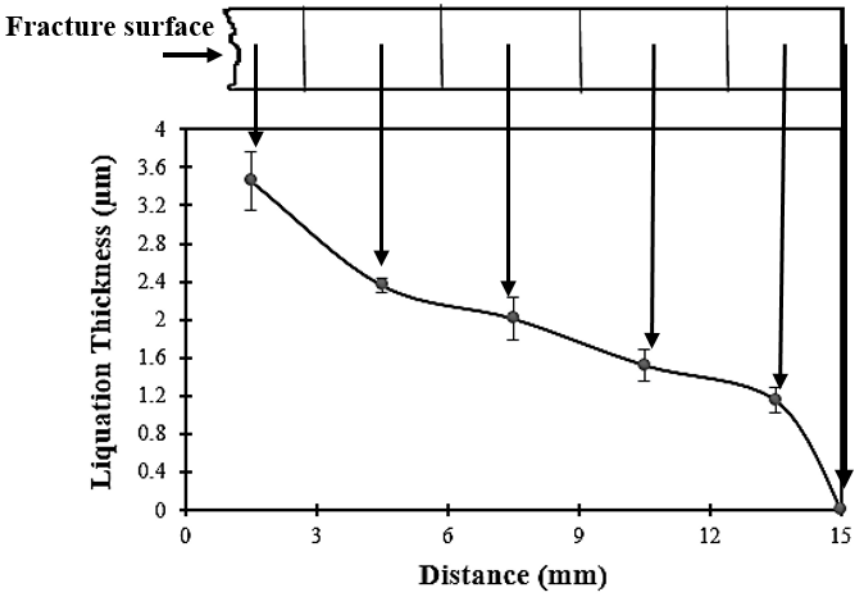

Figure 16. Variations of the liquation thickness from the fracture zone to the parent material in the sample. Obtained from the longitudinal cross section of the NDT test sample 1240°C. Measurements positions in the fractured sample are indicated by arrows.

Miller and Chadwick [59] studied on the effect of liquation on boundaries strength. They obtained the stress required for splitting the interface by overcoming surface tension at the solid-liquid interface on liquated grain boundaries (Eq. 5):

$$\sigma = \frac{2\gamma_{sl}}{h} \qquad \text{Eq. (5)}$$

Where the tensile stress, σ the stress required to overcome the attraction due to surface tension, γ_{sl} is surface tension at the solid-liquid interface and h is the liquid film thickness (the meniscus for the case of complete wetting is given by $\frac{h}{2}$). Furthermore, Xiao et al. [60] proposed the following equation to describe the evolution of the surface tension of an alloy with temperature [60]:

$$\gamma_{sl} = \gamma_l + k(T - T_L) \qquad \text{Eq. (6)}$$

Where γ_l, in mN/m, is the surface tension at liquidus temperature (T_L); k, in mN/(m.K), is the temperature coefficient of surface tension; and T is the temperature in Kelvin scale.

Equation (5) implies that the stress required separating the solid-liquid interface decreases with increasing thickness of the grain boundary liquid film. Accordingly, any factor that reduces the thickness (h) of the intergranular liquid film, it could presumably reduce the susceptibility of the alloy to cracking [61]. On the other hand, based on equations (4) and (6), the closer the temperature is to the liquidus, the lower will be the surface tension. Therefore, reduction in surface tension decreases the critical size for the formation of a void resulting in increased formation and coalescence of the voids and cavities. It should be noted, a very accurate calculation would require the determination of the surface tension of the AD730^{TM} alloy which is out of the scope of the present work.

Ojo et al. [6] and Lin et al. [62] reported that NDT usually occurs at the onset of grain boundary liquation, so the lower the GB liquation temperature the lower will be the NDT [6, 62]. Generally, any factor that reduces the temperature of grain boundary liquation initiated during the welding heating cycle, increases material's susceptibility to liquation cracking. In the present study, it was found that the intergranular carbide particles present in the AD730^{TM} superalloy decreased the liquation initiation temperature in the material and can be considered as the most detrimental phase in promoting cracking susceptibility. Similar results have been reported by Egbewande et al. [61] in IN738 and Montazeri et al. [5] in IN738LC that the melting and liquation of Cr-Mo rich carbides (or borides) at lower temperatures resulted in the higher susceptibility to liquation cracking with the effects being intensified by hard carbides such as MC (Ti, Mo, and Nb-rich) carbides.

The above findings demonstrate that, in addition to the voids and cavities, the formation of liquated zones at the grain boundaries, has a significant impact on the NDT point. Specifically,

liquation at the boundaries acts as an accelerating factor for the interconnection of cavities resulting in faster joining of the voids and cavities and the ensuing intergranular fracture. Evidently, faster damage is expected at higher temperatures due to the increased liquation at the boundaries and reduced surface tension between the grains.

4. Conclusions

Hot ductility behavior of the nickel base alloy AD730™ was investigated using Gleeble™ thermomechanical simulator. Different heating rates representative of those observed during linear friction welding were used. The microstructure and fracture surface of the samples were examined and the possible mechanisms responsible for the loss of ductility were proposed. The following conclusions can be made from this investigation:

1. The nil strength and nil ductility temperatures of the alloy were determined to be 1290°C and 1234°C, respectively.
2. Variation of heating rates from 5 to 100 °C/s does not have a significant influence on the NST point. However, this variation changed the size and fraction of voids in the fracture surface.
3. The failure mechanism at nil strength temperature seems to be mostly controlled by void nucleation and growth.
4. Liquation within the grain boundaries and the reduction in surface tension at the grain boundary-matrix interface combined with the presence of Nb and Mo rich MC appear to be the main mechanisms for ductility loss at the NDT point.
5. The nucleation, growth, and coalescence of cavities and voids occur during hot deformation and the extent of material damage is a function of temperature, applied stress, and time.

Acknowledgments

The authors would like to thank the support of the National Science and Engineering Council (NSERC, Canada) 2018-03889 through a Discovery Grant. Technical support provided by Dr. Mohammad Saadati for SEM work and Mr. Radu Romanica for Gleeble testing is very much appreciated.

References

[1] J.L.Caron, J.W.Sowards, Weldability of Nickel-Base Alloys, Comprehensive Materials Processing, Elsevier2014, pp. 151-179.
[2] S.T. Mandziej, Testing for Susceptibility to Hot Cracking on Gleeble™ Physical Simulator, Springer, Berlin, Heidelberg2005.
[3] Z. Huang, W.M. Shun, M. Yao, A method to estimate the nil-ductility transition temperature, Scripta Metallurgica et Materialia, 24, (4), (1990), 691-695. 10.1016/0956-716x(90)90225-6.
[4] C.-W. Li, A.-C. Yeh, C.-S. Chen, W.-R. Wang, Hot Ductility Loss in a Fe-Ni-Based Superalloy, Metals, 5, (4), (2015), 2428-2434. 10.3390/met5042428.

[5] M. Montazeri, F.M. Ghaini, The liquation cracking behavior of IN738LC superalloy during low power Nd:YAG pulsed laser welding, Materials Characterization, 67, (2012), 65-73. 10.1016/j.matchar.2012.02.019.
[6] O.A. Ojo, M.C. Chaturvedi, On the role of liquated γ′ precipitates in weld heat affected zone microfissuring of a nickel-based superalloy, Materials Science and Engineering: A, 403, (1-2), (2005), 77-86. 10.1016/j.msea.2005.04.034.
[7] Z.L. Zhao, Y.Q. Ning, H.Z. Guo, Z.K. Yao, M.W. Fu, Discontinuous yielding in Ni-base superalloys during high-speed deformation, Materials Science and Engineering: A, 620, (2015), 383-389. 10.1016/j.msea.2014.10.041.
[8] Y.C. Lin, J. Deng, Y.-Q. Jiang, D.-X. Wen, G. Liu, Hot tensile deformation behaviors and fracture characteristics of a typical Ni-based superalloy, Materials & Design, 55, (2014), 949-957. 10.1016/j.matdes.2013.10.071.
[9] J.-l. Qu, Z.-n. Bi, J.-h. Du, M.-q. Wang, Q.-z. Wang, J. Zhang, Hot Deformation Behavior of Nickel-Based Superalloy GH4720Li, Journal of Iron and Steel Research, International, 18, (10), (2011), 59-65. 10.1016/s1006-706x(12)60023-5.
[10] I. Mejía, A. Bedolla-Jacuinde, C. Maldonado, J.M. Cabrera, Hot ductility behavior of a low carbon advanced high strength steel (AHSS) microalloyed with boron, Materials Science and Engineering: A, 528, (13-14), (2011), 4468-4474. 10.1016/j.msea.2011.02.040.
[11] J. Andersson, G. Sjöberg, M.C. Chaturvedi, Hot Ductility Study of Haynes 282 Superalloy, in: J.R.G. E. A. Ott, A. Banik, I. Dempster, T. P. Gabb, R. Helmink, X. Liu, A. Mitchell, G. P. Sjöberg, and A. Wusa (Ed.) Proceeding of the 7th International Symposium on Superalloy 718 and Derivatives, TMS (The Minerals, Metals and Materials Society), 2010.
[12] R. Raj, M.F. Ashby, Intergranular fracture at elevated temperature, Acta Metallurgica, 23, (6), (1975), 653-666. 10.1016/0001-6160(75)90047-4.
[13] J.E. Ramirez, Susceptibility of IN740 to HAZ Liquation Cracking and Ductility-Dip Cracking, Welding Journal, 91, (4), (2012), 122s-131s.
[14] M. Qian, J.C. Lippold, Liquation phenomena in the simulated heat-affected zone of alloy 718 after multiple postweld heat treatment cycles, Welding Journal-New York, 82, (6), (2003), 145-150.
[15] F.F. Noecker, J.N. DuPont, Metallurgical Investigation into Ductility Dip Cracking in Ni-Based Alloys: Part II, Welding Journal, 88, (3), (2009), 62s-77s.
[16] M.J. Cieslak, J.J. Stephens, M.J. Carr, A study of the weldability and weld related microstructure of cabot alloy 214, Metallurgical Transactions A, 19, (3), (1988), 657–667. 10.1007/BF02649280.
[17] M. Qian, J.C. Lippold, The effect of multiple postweld heat treatment cycles on the weldability of Waspaloy (R), Welding Journal, 81, (11), (2002), 233s-238s.
[18] C.-R. Lee, S.-H. Um, S.-W. Kim, C. Choi, C.-H. Lee, A Study on Hot Ductility Behavior of Ni-based Superalloys, Journal of Welding and joining, 22, (2), (2004), 59-68.
[19] N.O. Knock, Characterization of Inconel 718: Using The Gleeble and Varestraint Testing Methods to Determine The Weldability of Inconel 718, Materials Engineering, California Polytechnic State University - San Luis Obispo, 2010.
[20] F. Masoumi, D. Shahriari, H. Monajati, J. Cormier, B.C.D. Flipo, A. Devaux, M. Jahazi, Linear friction welding of AD730™ Ni-base superalloy: Process-microstructure-property interactions, Materials & Design, 183, (2019), 10.1016/j.matdes.2019.108117.
[21] A. Chamanfar, M. Jahazi, J. Cormier, A Review on Inertia and Linear Friction Welding of Ni-Based Superalloys, Metallurgical and Materials Transactions A, 46, (4), (2015), 1639-1669. 10.1007/s11661-015-2752-4.
[22] M.M. Smith, Characterization of Linear Friction Welded In-Service Inoconel 718 Superalloy, Mechanical Engineering, The University of British Columbia (Okanagan), 2017.
[23] M. Smith, L. Bichler, D. Sediako, Measurement of Residual Stresses in Linear Friction Welded In-Service Inconel 718 Superalloy, Materials Science Forum, 879, (2016), 1800-1806. 10.4028/www.scientific.net/MSF.879.1800.
[24] M.E. Nunn, Aero engine improvements through linear friction welding, 1st International Conference on Innovation and Integration in Aerospace Sciences, CEIA, Queen's University Belfast, Northern Ireland, UK, 2005.
[25] A. Vairis, M. Frost, Modelling the linear friction welding of titanium blocks, Materials Science and Engineering: A, 292, (1), (2000), 8-17. 10.1016/s0921-5093(00)01036-4.
[26] C. Mary, M. Jahazi, Linear Friction Welding of IN-718 Process Optimization and Microstructure Evolution, Advanced Materials Research, 15-17, (2006), 357-362. 10.4028/www.scientific.net/AMR.15-17.357.
[27] J.L. Caron, J.W. Sowards, Weldability of Nickel-Base Alloys, in: S. Hashmi (Ed.), Comprehensive Materials Processing, Elsevier2014, pp. 151-179.

[28] A. Devaux, A. Helstroffer, J. Cormier, P. Villechaise, J. Douin, M. Hantcherli, F. Pettinari-Sturmel, Effect of aging heat-treatment on mechanical properties of AD730TM superalloy, TMS, 8th International Symposium on Superalloy 718 and Derivatives, John Wiley and Sons Inc., 2014, pp. 521-535.
[29] M. Pérez, C. Dumont, O. Nodin, S. Nouveau, Impact of forging direction on the recrystallization behaviour of nickel base superalloy AD730 billet material at subsolvus temperatures, Materials Characterization, 146, (2018), 169-181. 10.1016/j.matchar.2018.10.003.
[30] ASTM-International, ASTM E1382 - 97-Standard Test Methods for Determining Average Grain Size Using Semiautomatic and Automatic Image Analysis, 2015.
[31] M. Qian, An investigation of the repair weldability of Waspaloy and Alloy 718, Welding Engineering, The Ohio State University, 2001.
[32] G.A. Knorovsky, M.J. Cieslak, T.J. Headley, A.D. Romig, W.F. Hammetter, INCONEL 718: A solidification diagram, Metallurgical Transactions A, 20, (10), (1989), 2149-2158. 10.1007/bf02650300.
[33] C.P. Chou, C.H. Chao, Repair Weldability Studies of Alloy 718 Using Versatile varestraint Test, Superalloys 1988, The Metallurgical Society/AIME, 1988, pp. 785-794.
[34] F. Masoumi, D. Shahriari, M. Jahazi, J. Cormier, B.C.D. Flipo, On the Occurrence of Liquation During Linear Friction Welding of Ni-Based Superalloys, Metallurgical and Materials Transactions A, 48, (6), (2017), 2886-2899. 10.1007/s11661-017-4067-0.
[35] Y.C. Lin, J. Deng, Y.-Q. Jiang, D.-X. Wen, G. Liu, Effects of initial δ phase on hot tensile deformation behaviors and fracture characteristics of a typical Ni-based superalloy, Materials Science and Engineering: A, 598, (2014), 251-262. 10.1016/j.msea.2014.01.029.
[36] G.E. Dieter, Mechanical metallurgy, McGraw-Hill book company1988.
[37] F. Masoumi, D. Shahriari, M. Jahazi, J. Cormier, A. Devaux, Kinetics and Mechanisms of gamma' Reprecipitation in a Ni-based Superalloy, Scientific reports, 6, (2016), 28650. 10.1038/srep28650.
[38] F. Masoumi, M. Jahazi, J. Cormier, D. Shahriari, Dissolution kinetics and morphological changes of γ′ in AD730TMsuperalloy, MATEC Web of Conferences, 14, (2014), 10.1051/matecconf/20141413005.
[39] F. Masoumi, M. Jahazi, D. Shahriari, J. Cormier, Coarsening and dissolution of γ′ precipitates during solution treatment of AD730™ Ni-based superalloy: Mechanisms and kinetics models, Journal of Alloys and Compounds, 658, (2016), 981-995. 10.1016/j.jallcom.2015.11.002.
[40] F. Masoumi, L. Thébaud, D. Shahriari, M. Jahazi, J. Cormier, A. Devaux, B.C.D. Flipo, High temperature creep properties of a linear friction welded newly developed wrought Ni-based superalloy, Materials Science and Engineering: A, 710, (2018), 214-226. 10.1016/j.msea.2017.10.091.
[41] S. Davies, S. Jeffs, R. Lancaster, G. Baxter, High Temperature Deformation Mechanisms in a DLD Nickel Superalloy, Materials (Basel), 10, (5), (2017), 10.3390/ma10050457.
[42] Y. Sasajima, T. Akabane, T. Nagai, Y. Chonan, J. Onuki, Void generation during the annealing process of very narrow copper wires, Journal of Applied Physics, 105, (7), (2009), 10.1063/1.3091291.
[43] M.J. Mcnallan, T. Debroy, Effect of Temperature and Composition on Surface-Tension in Fe-Ni-Cr Alloys Containing Sulfur, Metall Trans B, 22, (4), (1991), 557-560. Doi 10.1007/Bf02654294.
[44] J.J. Jonas, C. Ghosh, X. Quelennec, V.V. Basabe, The Critical Strain for Dynamic Transformation in Hot Deformed Austenite, ISIJ International, 53, (1), (2013), 145-151. 10.2355/isijinternational.53.145.
[45] A.A. Guimaraes, J.J. Jonas, Recrystallization and aging effects associated with the high temperature deformation of waspaloy and inconel 718, Metallurgical Transactions A, 12, (9), (1981), 1655-1666. 10.1007/bf02643571.
[46] A. Chamanfar, M. Jahazi, J. Gholipour, P. Wanjara, S. Yue, Evolution of flow stress and microstructure during isothermal compression of Waspaloy, Materials Science and Engineering: A, 615, (2014), 497-510. 10.1016/j.msea.2014.07.093.
[47] X. Zhao, J. Chen, X. Lin, W. Huang, Study on microstructure and mechanical properties of laser rapid forming Inconel 718, Materials Science and Engineering: A, 478, (1-2), (2008), 119-124. 10.1016/j.msea.2007.05.079.
[48] Y. Huang, T.G. Langdon, Cavitation and failure in a fine-grained Inconel 718 alloy having potential superplastic properties, Materials Science and Engineering: A, 410-411, (2005), 130-133. 10.1016/j.msea.2005.08.095.
[49] J. Andersson, G.P. Sjöberg, L. Viskari, M. Chaturvedi, Effect of different solution heattreatments on hot ductility of superalloysPart 2 – Allvac 718Plus, Materials Science and Technology, 28, (6), (2013), 733-741. 10.1179/1743284712y.0000000002.
[50] O.T. Ola, O.A. Ojo, M.C. Chaturvedi, Effect of deformation mode on hot ductility of a γ′ precipitation strengthened nickel-base superalloy, Materials Science and Engineering: A, 585, (2013), 319-325. 10.1016/j.msea.2013.06.088.

[51] R.W. Hertzberg, Deformation And Fracture Mechanics of Engineering Materials, John Wiley & Sons1996.
[52] K. Aning, J.K. Tien, Creep and stress rupture behavior of a wrought nickel-base superalloy in air and vacuum, Materials Science and Engineering, 43, (1), (1980), 23-33. 10.1016/0025-5416(80)90203-7.
[53] R.C. Gifkins, Grain-boundary participation in high-temperature deformation: An historical review, Materials Characterization, 32, (2), (1994), 59-77. 10.1016/1044-5803(94)90093-0.
[54] J.N. Greenwood, Intercrystalline cracking of metals, Bull. Inst. Metals, 12, (1952), 104-105.
[55] H. Riedel, Fracture at high temperatures, Springer-Verlag, Berlin ; New York, 1987.
[56] R.W. Smith, D.J. Srolovitz, Void formation during film growth: A molecular dynamics simulation study, Journal of Applied Physics, 79, (3), (1996), 1448-1457. 10.1063/1.360983.
[57] J.R. Davis, Tensile Testing, ASM International2004.
[58] F. Xiao, L.-x. Liu, R.-h. Yang, H.-k. Zhao, L. Fang, C. Zhang, Surface tension of molten Ni-(Cr, Co, W) alloys and segregation of elements, Transactions of Nonferrous Metals Society of China, 18, (5), (2008), 1184-1188. 10.1016/s1003-6326(08)60202-2.
[59] W.A. Miller, G.A. Chadwick, On the magnitude of the solid/liquid interfacial energy of pure metals and its relation to grain boundary melting, Acta Metallurgica, 15, (4), (1967), 607-614. 10.1016/0001-6160(67)90104-6.
[60] Xiao Feng, Fang Liang, N. K., Surface tension and molten Ni and Ni-Co alloys, Journal of Materials Science and Technology, (2005), 201-206.
[61] A.T. Egbewande, H.R. Zhang, R.K. Sidhu, O.A. Ojo, Improvement in Laser Weldability of Incomel 738 Superalloy through Microstructural Modification, Metallurgical and Materials Transactions A, 40, (11), (2009), 2694-2704. 10.1007/s11661-009-9962-6.
[62] W. Lin, J.C. Lippold, W.A. Baeslack III, An evaluation of heat-affected zone liquation cracking susceptibility, Part I: Development of a method for quantification, Welding Journal, 72, (1993), 135–153.